

# Geostatistical modeling of riparian forest microclimate and its implications for sampling

Bianca N.I. Eskelson, Paul. D. Anderson, Joan C. Hagar, and Hailemariam Temesgen

**Abstract:** Predictive models of microclimate under various site conditions in forested headwater stream – riparian areas are poorly developed, and sampling designs for characterizing underlying riparian microclimate gradients are sparse. We used riparian microclimate data collected at eight headwater streams in the Oregon Coast Range to compare ordinary kriging (OK), universal kriging (UK), and kriging with external drift (KED) for point prediction of mean maximum air temperature ( $T_{air}$ ). Several topographic and forest structure characteristics were considered as site-specific parameters. Height above stream and distance to stream were the most important covariates in the KED models, which outperformed OK and UK in terms of root mean square error. Sample patterns were optimized based on the kriging variance and the weighted means of shortest distance criterion using the simulated annealing algorithm. The optimized sample patterns outperformed systematic sample patterns in terms of mean kriging variance mainly for small sample sizes. These findings suggest methods for increasing efficiency of microclimate monitoring in riparian areas.

**Résumé :** Les modèles de prédiction du microclimat pour différentes conditions de station dans les zones riveraines boisées des cours d'eau de tête de bassin sont peu développés et les procédures d'échantillonnage pour caractériser les gradients sous-jacents du microclimat riverain sont rares. Nous avons utilisé des données de microclimat riverain collectées le long de huit cours d'eau de tête de bassin dans la chaîne côtière de l'Oregon pour comparer le krigeage ordinaire (KO), le krigeage universel (KU) et le krigeage avec dérive externe (KDE) pour la prédiction localisée de la température moyenne maximale de l'air ( $T_{air}$ ). Plusieurs caractéristiques topographiques et de la structure de la forêt ont été considérées comme paramètres spécifiques à la station. L'élévation au-dessus du cours d'eau et la distance du cours d'eau étaient les covariables les plus importantes dans les modèles de KDE qui donnaient de meilleurs résultats que le KO et le KU en termes d'écart-type. La répartition des échantillons a été optimisée sur la base de la variance de krigeage et des moyennes pondérées du critère de la plus courte distance à l'aide d'un algorithme de recuit simulé. La répartition optimisée des échantillons donnait de meilleurs résultats que la répartition systématique en termes de variance moyenne de krigeage, surtout lorsque le nombre d'échantillons était faible. Ces résultats suggèrent des méthodes pour augmenter l'efficacité du suivi du microclimat dans les zones riveraines.

[Traduit par la Rédaction]

## Introduction

Microclimates are defined by local differences in environmental variables such as temperature, light, wind speed, and moisture close to the Earth's surface. Microclimates can vary on a scale of a few tens of metres, a few centimetres, or even a few millimetres, and such small-scale differences in climate are important to plants and animals (Adams 2007, p.79). Microclimates can be spatially and temporally dynamic in association with changes in ecosystem structure arising from natural processes such as vegetation growth, succession, and disturbance and anthropogenic factors such as forest management (Chen et al. 1999). Characterization of forest microcli-

matic gradients can help explain observed patterns in biodiversity, biogeochemical cycles, and other system-level processes (Naiman et al. 2000).

Microclimate gradients that traverse forest edges have been studied thoroughly (e.g., Chen et al. 1993, 1995; Geiger et al. 2003, section 37), whereas studies of forest riparian microclimate gradients have been undertaken only recently (Olson et al. 2007). Forest riparian microclimate is influenced by factors such as the stream channel (Moore et al. 2005), the topography near the interface between terrestrial and aquatic systems (Rambo and North 2008), and the hydrology and macroclimate of the area (Olson et al. 2007). The complexity of riparian microclimatic gradients produces great heteroge-

Received 7 September 2010. Accepted 21 January 2011. Published at [www.nrcresearchpress.com/cjfr](http://www.nrcresearchpress.com/cjfr) on 18 April 2011.

**B.N.I. Eskelson and H. Temesgen.** Oregon State University, Department of Forest Engineering, Resources and Management, 204 Peavy Hall, Corvallis, OR 97331-5706, USA.

**P.D. Anderson.** Biology and Culture of Forest Plants Team, U.S. Department of Agriculture Forest Service, Pacific Northwest Research Station, Corvallis, Oregon, USA.

**J.C. Hagar.** U.S. Geological Survey, Forest and Rangeland Ecosystem Science Center, Forestry Sciences Lab, 3200 SW Jefferson Way, Corvallis, OR 97331, USA.

**Corresponding author:** Bianca N.I. Eskelson (e-mail: [bianca.eskelson@oregonstate.edu](mailto:bianca.eskelson@oregonstate.edu)).

neity in processes and diversity of habitats and therefore has an important influence on fish and wildlife (Richardson et al. 2005). Forest management strategies such as the retention of streamside vegetation buffers may alter riparian microclimates (Chen et al. 1999) and affect stream conditions (e.g., stream temperature) (Olson et al. 2007).

Knowledge of the spatial distribution of microclimate conditions is required to meet management objectives for fish and wildlife habitats in streams and riparian buffers of headwater forests. Intensive sampling to determine spatial variation in microclimate can be impractical. Ability to predict microclimate conditions for unsampled locations within riparian buffers of headwater streams may obviate the need for intensive measurement. However, few studies have focused on modeling microclimate variables in forested landscapes (Vanwallegem and Meentemeyer 2009), and to our knowledge, none has addressed modeling of microclimate characteristics in riparian buffers of headwater streams.

Riparian microclimate data have typically been collected using transects across stream–riparian gradients (see table 1 in Olson et al. 2007) and therefore violate the independence assumption underpinning classical statistical approaches such as multiple linear regression. Geostatistical methods such as kriging provide a more flexible analytical approach that accommodates spatially autocorrelated data. In comparisons of kriging and regression techniques, kriging with external drift, which incorporates covariates other than spatial location, outperformed simple linear regression (soil metrics; Bourenne et al. 2000) and provided better forest temperature predictions than multiple regression (Vanwallegem and Meentemeyer 2009). Consequently, our interest was to assess the utility of different kriging approaches to model headwater riparian microclimate.

The effectiveness of predictive modeling depends largely on the quality of the underlying data (Stein and Ettema 2003). The sampling scheme impacts both the suitability of data for predictive modeling and the efficiency and costs of a survey (van Groenigen et al. 1999). Therefore, optimization of sampling intensity and spatial pattern for quantification of complex microclimate gradients in riparian buffers would increase the efficiency of efforts to monitor forest management impacts on riparian microclimate. Headwater streams of the Pacific Northwest typically exert the strongest effect on air temperature and relative humidity within 10 to 15 m of the stream channel (Rykken et al. 2007; Anderson et al. 2007). The spacing between microclimate sensors needs to be sufficient to quantify the nonlinear microclimate gradients at both the stream–buffer edge and the buffer–upslope edge (Olson et al. 2007). However, in most past studies, microclimate sensors have been placed at set intervals along a stream–riparian gradient. For example, Hagan and Whitman (2000) and Welsh et al. (2005) installed microclimate sensors every 10 m from the stream, whereas Brososke et al. (1997) and Dong et al. (1998) sampled microclimate at the stream center, the buffer edge, and at 15, 30, and 60 m upslope of the buffer edge. In contrast, Anderson et al. (2007) sampled microclimate with a higher intensity close to the stream than upslope (stream center, ~6, ~15, ~25, ~50 m, and at 20 m intervals beyond 50 m). To optimize sampling and long-term monitoring designs, search algorithms in combination with interpolation methods such as kriging are increasingly being

used in other fields. For example, Li and Chan Hilton (2005, 2007) optimized groundwater monitoring networks. In the terminology of this paper, Brus and Heuvelink (2007) optimized samples with kriging with external drift using the simulated annealing algorithm.

Our study objectives with respect to eight specific headwater stream reaches were as follows: (i) identify possible predictor variables for modeling mean daily maximum air temperature; (ii) compare the performance of ordinary kriging, universal kriging, and kriging with external drift in predicting mean daily maximum air temperature along transects from streamside to upslope; (iii) design an optimal sample pattern for microclimate sensors across riparian gradients based on the kriging variance and the weighted means of shortest distances criterion; and (iv) contrast the prediction performance of kriging based on the optimized sample patterns and random samples with the prediction performance of kriging based on a systematic sample pattern for a range of sample sizes.

## Methods

### Data

Microclimate data from eight headwater stream reaches (subsequently referred to as reach or reaches) were collected in 2006 at four sites of the Bureau of Land Management Density Management Study in the Coast Range of Oregon, USA (Table 1; for DMS details, see Cissel et al. 2006). Reach locations ranged from west of Corvallis to north of Roseburg, Oregon, USA (range 43°17'30"N to 44°31'41"N, 122°27'55"W to 123°41'11"W).

A sampling block (72 m × 72 m horizontal distance) was randomly located along each reach. One 72 m axis of the block was oriented approximately parallel to the stream; the center of the block along this axis will be referred to as the center line (CL). The second axis extended approximately 36 m (horizontal distance) upslope and perpendicular to the CL on each side of the stream (Fig. 1). Microclimate sensors were positioned along four transects. Transects with 3 m horizontal spacing were laid out perpendicular to the CL at the 32 and 68 m marks of the CL. Transects with 10 m horizontal spacing were laid out perpendicular to the CL at two random points between 0 and 72.

Air temperature at 1 m above the ground was measured using three-channel humidity and dual-temperature data loggers (models GPSE 101 203 and GPSE 301 203, A.R. Harris Ltd., Christchurch, New Zealand). The data loggers were attached to fiberglass rods inserted into the ground, and ventilated plastic cups were suspended over each data logger to prevent direct exposure to the sun. Because of the limited number of available sensors, microclimate monitoring rotated among the eight reaches between 19 July and 11 September 2006 (see Table 1), with sensors deployed three to seven (median = 5) consecutive days at each site. Sensors at each transect position (Fig. 1) recorded microclimate values every 20 min. The data were initially reduced to hourly mean values. Subsequently, mean daily estimates of the maximum hourly air temperature ( $T_{\text{air}}$ ) values were computed for each sampled location. For the seven of eight reaches that were sampled on four or more days, daily maximum temperature values were averaged across all sensors to identify the three

**Table 1.** General information on the eight headwater sites.

Site	BLM district	Latitude (N)	Longitude (W)	Elevation (m)	Density	Buffer	Stream slope (%)	Streamside slope (%)	Aspect of channel orientation (°)	Date in 2006 of microclimate measurements
Keel Mountain, reach 17 (KM17)	Salem	44°31'41.0"	122°37'55.0"	700	Control	Control	17	12	266	29–31 August
Ten High, reach 46 (TH46)	Eugene	44°16'50.0"	123°31'06.0"	525	Control	Control	16	22	92	8–16 August
Keel Mountain, reach 18 (KM18)	Salem	44°31'41.0"	122°37'55.0"	745	Moderate	Two site potential tree heights	20	21	269	19–24 July
Keel Mountain, reach 19 (KM19)	Salem	44°31'41.0"	122°37'55.0"	730	Moderate	Two site potential tree heights	25	20	230	15–23 August
Bottom Line, reach 13 (BL13)	Eugene	43°46'20.0"	123°14'11.0"	295	Moderate	Two site potential tree heights	18	66	323	5–11 September
Keel Mountain, reach 21 (KM21)	Salem	44°31'41.0"	122°37'55.0"	670	Moderate	Variable width	10	43	265	24–29 August
Ten High, reach 75 (TH75)	Eugene	44°16'50.0"	123°31'06.0"	520	Moderate	Variable width	60	40	173	1–7 August
OM Hubbard, reach 36 (OM36)	Roseburg	43°17'30.0"	123°35'00.0"	510	Moderate	Variable width	19	40	71	12–19 September

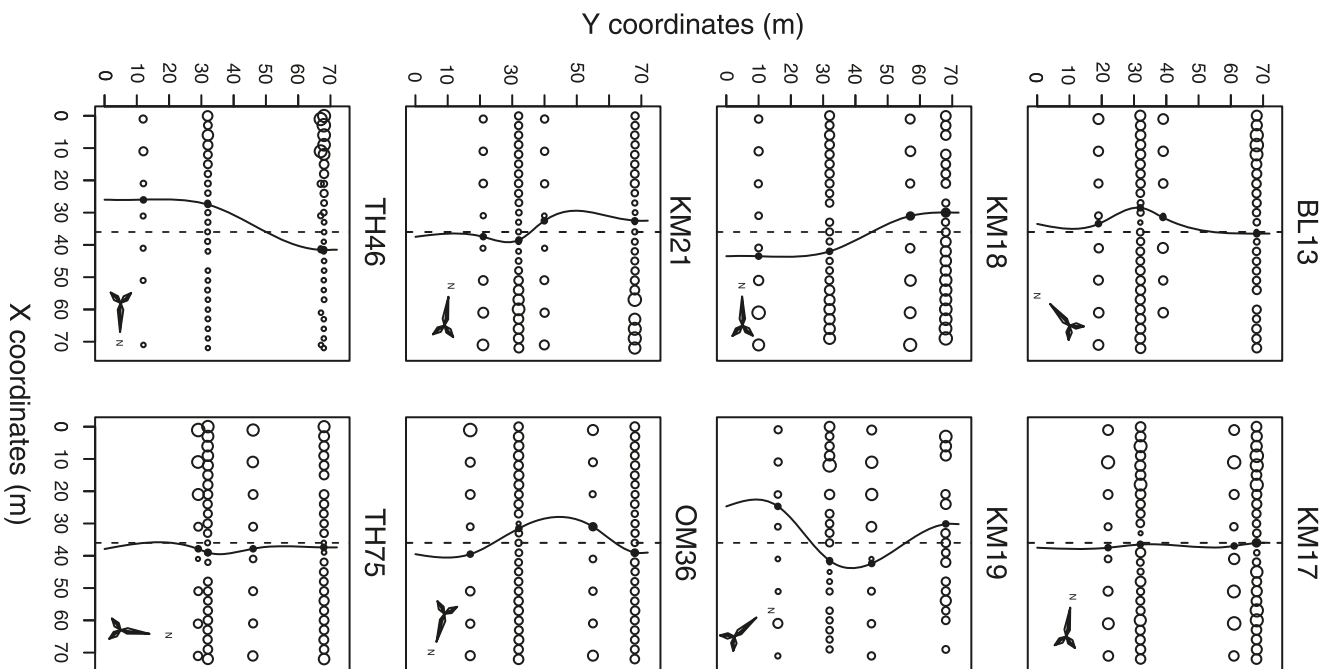


**Fig. 1.** Locations of the microclimate sensors at the eight stream reaches: open circle, microclimate sensor location, size proportional to observed  $T_{air}$  within site; solid circle, observed stream location; the center line is represented by the broken line; the spline interpo-lated stream course is represented by the solid line. See Table 1 for descriptions of stream reaches.

consecutive days having the greatest running average. Aver-aged daily maximum air temperature values for these three-day periods were the basis of the modeling presented here. A small proportion of the data loggers failed, resulting in dif-ferent numbers of  $T_{air}$  observations at each reach. Because the eight reaches were not concurrently sampled, they were mod-eled separately.

Several topographic and forest structure characteristics were investigated as possible contributors to spatial variation in microclimate. The horizontal distance to the stream (DTS, m) and the height above the stream (HAS, m) were recorded for each sensor position. DTS and HAS reflected existing knowledge of gradients in microclimate that occur laterally from stream to upslope (e.g., Brosofske et al. 1997; Anderson et al. 2007). The combination of DTS and HAS indicates the degree of stream channel incision. Log transformations of DTS and HAS were calculated as  $\ln(\text{DTS}) = \ln(\text{DTS} + 0.1)$  and  $\ln(\text{HAS}) = \ln(\text{HAS} + 5)$ , respectively, which linearized their relationship with  $T_{\text{air}}$  for some of the eight reaches. Measures of stand basal area and canopy leaf area index (LAI) were considered as indices of forest canopy interception of incident solar radiation (insolation) and therefore a limit to heat loading (Russell et al. 1989). Canopy cover also serves to insulate the channel microclimate from air exchange and therefore to maintain a near-stream humidity and cooler air mass. LAI ( $\text{m}^2$  foliage/ $\text{m}^2$  ground) and the diffuse non-interceptance (DIFN), defined as the proportion of visible sky, were measured at each microclimate sensor location using hemispherical detection of canopy light transmittance (plant canopy analyzer, model LAI-2000, LI-COR Biosciences, Lincoln, Nebraska). At the same points, the overstory density measures of trees per hectare (TPH) and basal area per hectare (BA/ha, in  $\text{m}^2/\text{ha}$ ) were calculated based on a variable radius plot with basal area factor 8. Percent (%) cover of forbs, ferns, low shrubs (<1.4 m), and tall shrubs (>1.4 m) were visually determined on 1 m  $\times$  1 m plots with the microclimate sensors at the plot center.

DTS was expected to have a consistent spatial influence on microclimate. At a finer spatial scale, we hypothesized that spatial variation in canopy density and, therefore, insolation interact with topography to locally influence microclimate based on characterizations of vegetation patterns in riparian zones (e.g., Pabst and Spies 1998; Hibbs and Bower 2001). To quantify the relationship between  $T_{\text{air}}$  and the available covariates, Pearson's correlation coefficient was calculated.

### Kriging

Kriging is a geostatistical approach that provides best linear unbiased predictions of the variable of interest,  $Z$ , at a location,  $\mathbf{s}_0$ , using the values  $z_i$  observed at neighboring locations  $\mathbf{s}_i$ . A large number of kriging methods exist (see Goovaerts 1997, pp. 125–258). Ordinary kriging (OK) does not allow for trend, whereas universal kriging (UK) incorporates the spatial coordinates as a linear or quadratic function in a trend model. Kriging with external drift (KED) allows the inclusion of additional covariates in the trend model, which in our study can account for the stream–riparian gradient in microclimate variables.

When the mean value of the variable of interest is assumed to be an unknown constant, kriging is called OK (Goovaerts 1997, p. 132; de Gruijter et al. 2006, p. 285). The predictions are based on the following model:

$$[1] \quad Z(\mathbf{s}) = \mu + \varepsilon'(\mathbf{s})$$

where  $\mu$  is the constant stationary function or global mean and  $\varepsilon'(\mathbf{s})$  is the spatially correlated stochastic part of the variation (Hengl 2007). The OK predictions are made as follows:

$$[2] \quad \widehat{z}_{\text{OK}}(\mathbf{s}_0) = \sum_{i=1}^n w_i(\mathbf{s}_0) \cdot z(\mathbf{s}_i) = \boldsymbol{\lambda}_0^T \cdot \mathbf{z}$$

where  $\boldsymbol{\lambda}_0^T$  is the transpose of the vector of kriging weights ( $w_i$ ), and  $\mathbf{z}$  is the vector of  $n$  observations (Hengl 2007).

$Z$  at some location  $\mathbf{s}_0$  can be modeled as the sum of a deterministic component, the drift (i.e., covariate), and a stochastic component:

$$[3] \quad Z(\mathbf{s}) = m(\mathbf{s}) + \varepsilon'(\mathbf{s})$$

where the drift  $m(\mathbf{s})$  is the deterministic part and the stochastic component  $\varepsilon'(\mathbf{s})$  accounts for the fluctuations around the drift (Bourenane and King 2003). In KED, the drift  $m(\mathbf{s})$  is defined externally as a linear function of covariates (Bourenane et al. 2000), and the predictions are made as follows:

$$[4] \quad \widehat{z}_{\text{KED}}(\mathbf{s}_0) = \sum_{i=1}^n w_i^{\text{KED}}(\mathbf{s}_0) \cdot z(\mathbf{s}_i) = \boldsymbol{\delta}_0^T \cdot \mathbf{z}$$

for

$$[5] \quad \sum_{i=1}^n w_i^{\text{KED}}(\mathbf{s}_0) \cdot q_k(\mathbf{s}_i) = q_k(\mathbf{s}_0), \quad k = 1, \dots, p$$

where  $z$  is the variable of interest,  $q_k$  represents the covariates,  $\boldsymbol{\delta}_0^T$  is the transpose of the vector of KED weights ( $w_i^{\text{KED}}$ ),  $p$  is the number of covariates, and  $\mathbf{z}$  is the vector of  $n$  observations (Hengl 2007).

UK is a special case of KED in which the drift is represented as a linear combination of the coordinates. For UK, the covariates  $q_k$  in eq. 5 are coordinates only. UK was performed with linear and quadratic trends to predict  $T_{\text{air}}$ . For KED, all available covariates were used as external drift individually and in combination with HAS and DTS. For a detailed description of OK, UK, and KED, see, for example, Goovaerts (1997, pp. 132, 139, and 194, respectively) or Hengl (2007).

Kriging requires prior knowledge of the model of spatial variation. Using all available observations of  $T_{\text{air}}$  for each of the eight sites, we first estimated the variogram parameters (partial sill, range, and nugget) of a spherical variogram model for each site separately by applying the methods-of-moments with weighted least squares (de Gruijter et al. 2006, pp. 173–174). With these parameter estimates as starting values, restricted maximum likelihood (REML) estimation was used to obtain estimates of the partial sill, range, and nugget parameters without bias (see Lark and Webster 2006). The REML estimates were then employed in the kriging approaches.

### Validation of kriging methods

The performance of the kriging methods was compared using leave-one-out cross-validation, where one microclimate observation at a time was temporarily removed from the data set and its value was predicted from the remaining  $n - 1$  observations using OK, UK, and KED with different external drift variables. The performance of each kriging method was assessed with the mean error (ME) and root mean square error (RMSE) defined as follows:



$$[6] \quad \text{ME} = \frac{1}{n} \sum_{i=1}^n (z_i - \hat{z}_i)$$

$$[7] \quad \text{RMSE} = \sqrt{\frac{1}{n} \sum_{i=1}^n (z_i - \hat{z}_i)^2}$$

where  $z_i$  is the observed  $T_{\text{air}}$  value and  $\hat{z}_i$  is the predicted  $T_{\text{air}}$  value.

For unbiased methods, ME should be close to zero. Two-sided  $t$  tests were performed to determine whether ME differed significantly from zero for the different models. RMSE should be small for accurate predictions and is expressed as percentage of the observed mean  $T_{\text{air}}$ .

All statistical analyses were performed in R (R Development Core Team 2009). The geoR package (Ribeiro and Diggle 2001) was used to execute OK, UK, and KED.

### Optimization of sampling locations

de Gruijter et al. (2006, p.132) recommended purposive sampling over probability sampling for model-based mapping. When the variogram is known or can be estimated, geostatistical samples can be used to optimize the sampling locations (de Gruijter et al. 2006, p. 149), which is typically done by minimizing either the mean or maximum kriging variances (de Gruijter et al. 2006, p. 155). van Groenigen et al. (1999) employed the simulated annealing algorithm to optimize spatial soil sample patterns by minimizing the mean OK variance, whereas Brus and Heuvelink (2007) made use of the simulated annealing algorithm to obtain an optimized sample pattern with minimum kriging variance. When information about the variogram is unavailable, spatial coverage sampling is an attractive alternative to geostatistical sampling (de Gruijter et al. 2006, p. 133). Walvoort et al. (2010) developed an R package for designing spatial coverage samples by minimizing the mean squared shortest distance using  $k$ -mean algorithm. van Groenigen and Stein (1998) minimized the mean shortest distance by the simulated annealing algorithm. van Groenigen et al. (2000) extended this approach by minimizing the weighted means of shortest distance (WMSD) criterion, which includes a weighting function based on prior knowledge that allows for more intense sampling in subareas with high priority.

In this study, sampling locations were optimized using the kriging variance (KVAR) and the WMSD criterion for each of the eight reaches for sample sizes ( $m$ ) ranging from 15 to 25. For KVAR, the sample pattern was chosen that had the smallest mean kriging variance for a given  $m$ . The kriging variance at  $s_0$  for kriging with external drift is as follows:

$$[8] \quad \hat{\sigma}_{\text{KED}}^2(s_0) = c(0) - \mathbf{c}_0^T \mathbf{C}^{-1} \mathbf{c}_0 + (\mathbf{q}_0 - \mathbf{q}^T \mathbf{C}^{-1} \mathbf{c}_0)^T (\mathbf{q}^T \mathbf{C}^{-1} \mathbf{q})^{-1} (\mathbf{q}_0 - \mathbf{q}^T \mathbf{C}^{-1} \mathbf{c}_0)$$

where  $c(0)$  is the constant variance of  $\varepsilon(\mathbf{s})$ ,  $\mathbf{c}_0$  is the vector of covariances of residuals at the prediction location and sampling locations,  $\mathbf{C}$  is the variance-covariance matrix of the residuals at the sampling locations,  $\mathbf{q}_0$  is a vector of covariates at the prediction location, and  $\mathbf{q}$  is the matrix of covariates at the  $m$  sampling locations (Hengl 2007; Müller 2007, p. 15). The sampling locations that minimized the mean kriging

variance were found by employing the simulated annealing algorithm (for details on the simulated annealing algorithm, see Reeves 1993).

For WMSD, the simulated annealing algorithm was employed to obtain the sampling locations that minimize the WMSD criterion for a given  $m$ . Locations within 15 m of the stream received a larger weight than locations farther away from the stream, resulting in more intensive sampling close to the stream. The WMSD criterion for a sample  $\mathbf{S}$  is given as

$$[9] \quad \varphi_{\text{WMSD}}(\mathbf{S}) = \sum_{j=1}^{n-m} \frac{w_j \cdot d(s_j, \mathbf{S})}{(n-m)}$$

where  $d(s_j, \mathbf{S})$  is the Euclidean distance from the  $j$ th evaluation point ( $s_j$ ) to the closest sample point of the sample  $\mathbf{S}$ ,  $n-m$  is the number of evaluation points where  $n$  is the number of available observations at a specific site, and

$$w_j = \begin{cases} 2 & \text{for DTS} \leq 15 \text{ m} \\ 1 & \text{for DTS} > 15 \text{ m} \end{cases}$$

is the weight given to the locations based on their distance to the stream (van Groenigen et al. 2000). The WMSD-optimized samples are based only on the distances among sample and evaluation points, whereas the KVAR-optimized samples rely on the performed kriging and the estimated variogram parameters.

In addition to the optimized sampling locations, random (RAND) and systematic (SYST) samples were taken at each reach for each  $m = 15$  to 25. All systematic samples included four evenly spaced sample points on the 10 m transects, and the remaining sample points were evenly distributed along the 3 m transects.

Kriging was performed for the eight reaches based on the samples selected for each of the four sampling methods (KVAR, WMSD, RAND, and SYST) for each  $m = 15$  to 25. The kriging model that performed best for specific reach was chosen (see Table 4). To compare the kriging results based on the four different sample patterns for each reach, the comparison had to be based on the same evaluation points. SYST was compared with the other three sample patterns (KVAR, WMSD, and RAND) by calculating the mean kriging variance (MeanV) for each method based only on the evaluation points that were identical for SYST and the other sample pattern for a given sample size  $m$ . This allowed a comparison of MeanV<sub>other</sub> of each sampling method (KVAR, WMSD, and RAND) with MeanV<sub>SYST</sub> of the SYST sample, and the relative efficiency (RE) could be calculated as follows:

$$[10] \quad \text{RE} = \frac{\text{MeanV}_{\text{other}}}{\text{MeanV}_{\text{SYST}}}$$

where  $\text{RE} > 1$  means that the SYST sample was more efficient than the other sample pattern with which it was compared, whereas for  $\text{RE} < 1$ , SYST was less efficient than the other sample pattern. The RE values of the four sample patterns were plotted across the sample sizes  $m = 15$  to 25 for each of the eight reaches. Because the result of RAND depends on the sample drawn, 200 random samples were drawn and the average MeanV over the 200 samples (see de Gruijter et al. 2006, p. 19) was compared with MeanV<sub>SYST</sub>.

**Results**

Species composition, forest structure, and topography, as well as  $T_{air}$ , varied greatly among the eight reaches. Reaches KM17 and OM36 had far smaller mean  $T_{air}$  (13.7 and 16.2 °C, respectively) than the other six reaches for which mean  $T_{air}$  ranged between 23.6 and 28.9 °C (Table 2). Mean fern and low shrub covers were greater than 25% for the sites with steep streamside slope and less than or equal to 25% for the sites with moderate streamside slope (Tables 1 and 2). A similar trend was observed for the mean cover of tall shrubs, which tended to be greater ( $\geq 16\%$ ) for reaches with steep streamside slope than for those with moderate streamside slope ( $\leq 23\%$ ). Reaches with greater understory vegetation cover (BL13, KM21, OM36, and TH75) exhibited greater DIFN ( $\geq 0.05$ ) and smaller LAI ( $\leq 4.33$ ) values than those with less understory vegetation cover (DIFN  $\leq 0.05$ , LAI  $\geq 4.06$ ; KM17, KM18, KM19, and TH46).

**Correlations between  $T_{air}$  and the covariates**

Several correlations between  $T_{air}$  and the covariates were apparent (Table 3). Except for one reach, significant correlation existed between  $T_{air}$  and DTS at the 5% level. HAS was significantly correlated with  $T_{air}$  on all sites. For three sites, the range of  $T_{air}$  was small on the north side of the stream and large on the south side (see Fig. 1). LAI showed significant negative correlation with  $T_{air}$  for six of the eight reaches, and DIFN showed significant positive correlation with  $T_{air}$  for four of the eight reaches. The overstory density variables (BA/ha, TPH) were significantly correlated with  $T_{air}$  on more reaches than the understory percent cover variables. The correlation between  $T_{air}$  and the overstory and understory cover variables was positive for some reaches and negative for others.

**Kriging**

For KED, only the models that provided one of the three lowest RMSE values for at least one of the reaches are presented (Table 4). For two reaches, the log transformation of DTS provided smaller RMSE values than untransformed DTS. For four reaches, the log transformation of HAS provided smaller RMSE values than the untransformed HAS. For these reaches, log transformations  $\ln(DTS + 0.1)$  and  $\ln(HAS + 5)$  were used for the KED models, whereas the untransformed data were used for the remaining reaches. UK with quadratic trend provided the best and third best results in terms of RMSE for two reaches. For all reaches, the best KED model outperformed the predictions of the OK and UK with linear trend models in terms of RMSE. KED models that included DTS or  $\ln(DTS + 0.1)$  as external drift outperformed KED models that included HAS or  $\ln(HAS + 5)$  as external drift in terms of RMSE for half the reaches.  $T_{air}$  predictions were more accurate for models including HAS or  $\ln(HAS + 5)$  as external drift instead of DTS or  $\ln(DTS + 0.1)$  for the remaining four reaches.

Understory cover covariates tended to be more significant in the KED models for reaches with large DIFN values (BL13, KM21, OM36, TH75), whereas overstory cover variables tended to be more significant in KED models for reaches with smaller DIFN values (KM17, KM18, KM19, TH46).

**Table 2.** Summary statistics of the mean (standard deviation in parentheses) maximum air temperature ( $T_{air}$ ) and the covariates for the eight stream reaches. See Table 1 for descriptions of reaches.

Covariates	BL13 (n = 64)	KM17 (n = 65)	KM18 (n = 61)	KM19 (n = 50)	KM21 (n = 65)	OM36 (n = 65)	TH46 (n = 62)	TH75 (n = 64)
$T_{air}$ (°C)	23.71 (1.43)	13.69 (0.36)	28.93 (1.14)	23.55 (0.87)	25.78 (4.21)	16.16 (0.53)	25.88 (3.54)	25.44 (1.42)
DTS	19 (11.5)	17 (10.9)	18.9 (11.6)	18.8 (11.9)	19 (11.3)	18.1 (11.2)	19.7 (12.4)	19.3 (11.2)
HAS	10 (6.6)	3.3 (2.9)	3.7 (3.5)	1.2 (2.7)	8.5 (4.8)	5.8 (4.2)	3.2 (2.8)	7.9 (4.8)
LAI	3.69 (0.66)	4.95 (0.59)	5.37 (0.54)	5.42 (0.74)	4.33 (0.95)	2.72 (0.86)	4.06 (0.87)	3.73 (0.91)
DIFN	0.06 (0.04)	0.02 (0.01)	0.02 (0.02)	0.02 (0.02)	0.05 (0.06)	0.13 (0.1)	0.05 (0.05)	0.07 (0.07)
BA/ha	54.63 (34.93)	94.15 (46.17)	83.41 (34.39)	48 (27.76)	52.92 (27.59)	43.94 (28)	83.48 (35.41)	71.5 (44.16)
TPH	377 (255)	624 (350)	861 (635)	500 (467)	485 (425)	499 (342)	528 (270)	659 (654)
% Low shrubs	45 (27)	14 (17)	24 (27)	22 (24)	30 (22)	42 (29)	17 (21)	34 (24)
% Tall shrubs	29 (36)	23 (29)	9 (15)	17 (24)	26 (28)	16 (26)	2 (5)	26 (35)
% Forbs	6 (9)	16 (18)	9 (19)	17 (16)	14 (16)	16 (20)	7 (14)	3 (6)
% Ferns	45 (28)	20 (23)	10 (15)	25 (23)	29 (28)	25 (31)	11 (17)	29 (26)

**Note:** DTS, distance to stream (m); HAS, height above stream (m); LAI, leaf area index (m<sup>2</sup> foliage/m<sup>2</sup> ground); DIFN, proportion visible sky; BA/ha, basal area per hectare (m<sup>2</sup>/ha); TPH, trees per hectare.

Can. J. For. Res. Downloaded from www.nrcresearchpress.com by OREGON STATE UNIVERSITY on 05/06/11 For personal use only.

**Table 3.** Pearson's correlation coefficient between the mean maximum air temperature ( $T_{\text{air}}$ ) and the covariates for the eight stream reaches. See Table 1 for descriptions of reaches.

Covariates	BL13 ( <i>n</i> = 64)	KM17 ( <i>n</i> = 65)	KM18 ( <i>n</i> = 61)	KM19 ( <i>n</i> = 50)	KM21 ( <i>n</i> = 65)	OM36 ( <i>n</i> = 65)	TH46 ( <i>n</i> = 62)	TH75 ( <i>n</i> = 64)
DTS	<b>0.72</b>	<b>0.43</b>	<b>0.59</b>	0.28	<b>0.70</b>	<b>0.74</b>	<b>0.40</b>	<b>0.83</b>
ln(DTS + 0.1)	<b>0.81</b>	<b>0.43</b>	<b>0.60</b>	0.26	<b>0.72</b>	<b>0.71</b>	<b>0.36</b>	<b>0.85</b>
HAS	<b>0.59</b>	<b>0.34</b>	<b>0.84</b>	<b>0.72</b>	<b>0.73</b>	<b>0.74</b>	<b>0.51</b>	<b>0.59</b>
ln(HAS + 5)	<b>0.73</b>	<b>0.32</b>	<b>0.84</b>	<b>0.47</b>	<b>0.74</b>	<b>0.61</b>	<b>0.41</b>	<b>0.63</b>
LAI	<b>-0.26</b>	<b>-0.55</b>	-0.21	<b>-0.39</b>	<b>-0.53</b>	<b>-0.44</b>	<b>-0.89</b>	-0.23
DIFN	0.09	<b>0.33</b>	-0.01	0.24	<b>0.38</b>	<b>0.36</b>	<b>0.80</b>	0.22
MTA	<b>-0.31</b>	-0.15	<b>-0.25</b>	0.16	<b>-0.35</b>	<b>0.46</b>	0.25	<b>0.39</b>
BA/ha	-0.08	<b>0.60</b>	<b>0.31</b>	-0.10	<b>-0.40</b>	-0.14	<b>0.51</b>	<b>-0.35</b>
TPH	-0.17	<b>0.33</b>	<b>0.31</b>	<b>-0.42</b>	-0.14	-0.18	<b>0.51</b>	<b>-0.39</b>
% Low shrubs	<b>0.57</b>	0.09	<b>0.45</b>	<b>0.36</b>	-0.02	0.20	-0.02	<b>0.27</b>
% Tall shrubs	-0.18	<b>-0.35</b>	<b>0.31</b>	0.27	-0.07	<b>-0.31</b>	-0.10	0.22
% Forbs	<b>0.26</b>	-0.16	<b>-0.30</b>	-0.05	<b>-0.38</b>	0.09	0.18	0.22
% Ferns	<b>-0.44</b>	0.12	0.08	0.01	0.16	-0.02	-0.08	-0.24

**Note:** DTS, distance to stream (m); HAS, height above stream (m); LAI, leaf area index ( $\text{m}^2$  foliage/ $\text{m}^2$  ground); DIFN, proportion visible sky; BA/ha, basal area per hectare ( $\text{m}^2/\text{ha}$ ); TPH, trees per hectare. Values in bold indicate significant linear coefficient of correlation at the 5% level.

ME values did not differ significantly from zero for any of the models (all  $p$  values > 0.48), meaning that all models provided unbiased predictions. Therefore, ME values are not presented.

### Optimization of sampling locations

The KVAR, WMSD, and RAND sample patterns were compared with the SYST sample in terms of RE. The RE values for RAND were greater than 1 for all sample sizes  $m$  for six of the reaches (Fig. 2). For KM21 and OM36, the RE values for RAND were less than 1 for  $m = 15$  (Fig. 2).

The RE values of both KVAR and WMSD tended to be less than one, hence exceeding the efficiency of SYST, for sample sizes  $m \leq 23$  and  $m \leq 22$ , respectively (Fig. 2). The largest improvement in efficiency over SYST tended to occur for small sample sizes,  $m \leq 20$  (Fig. 2). The RE values of KVAR tended to be slightly smaller than the RE values of WMSD for most sample sizes.

SYST sample points were allocated so that there were always four sample points on each of the two 10 m transects and the remaining sample points were distributed evenly across the 3 m transects. Therefore, SYST always resulted in sample points across all four transects. For small sample sizes ( $m \leq 20$ ), KVAR and WMSD mostly resulted in sample locations on only three of the four transects. If the fourth transect had sample points, these were typically within 15 m of the stream (Fig. 3, example for BL13). For larger sample sizes ( $m > 20$ ), KVAR and WMSD also resulted in sample points across all four transects.

### Discussion

This is the first study to apply kriging methods for predicting microclimate attributes in riparian zones and to explore the efficiency of different sample patterns for the deployment of microclimate sensors. Incorporating selected topographic and stand structure characteristics into kriging models improved their predictive ability. Optimized sample patterns ex-

hibited a potential to improve kriging predictions compared with systematic samples.

### Correlations between $T_{\text{air}}$ and the covariates

High variability in the correlations between  $T_{\text{air}}$  and the covariates across the eight reaches was likely due in part to asynchronous sampling. Because the microclimate sensors were not concurrently deployed across the eight reaches,  $T_{\text{air}}$  was not calculated for the same three days and ranged from July to September among the reaches (Table 1). Although the three hottest days were chosen from the available data at each reach, the relationships between  $T_{\text{air}}$  and the available environmental covariates might differ at the reaches simply because of the different times at which the air temperatures were recorded. This may explain the lower mean  $T_{\text{air}}$  values for KM17 and OM36 compared with the other reaches. Additional research is warranted to quantify changes in the gradient of  $T_{\text{air}}$  from the wet stream channel to the dry upslope during the summer months, and to determine whether the relationships between  $T_{\text{air}}$  and the available covariates change over this time period.

We observed an impact on the correlation coefficients between  $T_{\text{air}}$  and DTS for reaches in which  $T_{\text{air}}$  differed widely between the two sides of the stream. This differential behavior of  $T_{\text{air}}$  was observed for three reaches (KM18, KM21, and TH46) and can be attributed to the approximate east–west stream orientation (sensu Gomi et al. 2006; Webb et al. 2008). All three sites exhibited higher mean  $T_{\text{air}}$  and a higher range in  $T_{\text{air}}$  on the side south of the stream, whereas large changes in  $T_{\text{air}}$  with increasing distance from the stream did not occur on the northern side of the stream. However, this extreme difference in behavior of  $T_{\text{air}}$  on the north and south sides of the stream was not observed at the similarly oriented KM17. This could be explained by lower slope on the south side of this reach compared with the other three. These results suggest that in some cases predictions may be more accurate if stream sides were modeled separately. We were unable to do this because of the small number of available observations, but we recommend that future research explores



**Table 4.** Root mean square error (RMSE) of the mean maximum air temperature for the eight stream reaches. See Table 1 for descriptions of reaches.

Kriging method	Trend	% RMSE							
		BL13	KM17	KM18	KM19	KM21	OM36	TH46	TH75
OK		3.279	<b>1.938</b>	1.524	2.364	5.759	2.313	<b>3.437</b>	2.632
UK	quadratic	3.314	1.989	1.764	2.361	5.692	<b>2.248</b>	3.722	<b>2.457</b>
KED	~coords + HAS	2.836	<b>1.935</b>	<b>1.445</b>	<b>2.158</b>	5.188	2.322	3.559	2.909
KED	~coords + HAS + LAI	3.03	1.941	<b>1.470</b>	<b>2.204</b>	<b>5.020</b>	2.297	3.691	2.832
KED	~coords + HAS + DIFN	2.966	1.955	1.504	2.233	<b>5.077</b>	2.323	<b>3.303</b>	2.82
KED	~coords + HAS + TPH	2.783	<b>1.925</b>	1.486	2.255	5.275	2.294	3.530	3.03
KED	~coords + HAS + Tall shrubs	2.996	1.955	1.482	<b>2.222</b>	5.241	<b>2.248</b>	3.448	2.78
KED	~coords + HAS + Ferns	2.917	1.945	<b>1.456</b>	2.226	<b>4.796</b>	2.281	3.485	2.809
KED	~coords + DTS	<b>2.574</b>	1.988	1.618	2.243	5.463	2.275	3.606	<b>2.501</b>
KED	~coords + DTS + DIFN	<b>2.600</b>	2.003	1.626	2.409	5.465	2.291	<b>3.020</b>	2.521
KED	~coords + DTS + TPH	<b>2.566</b>	1.97	1.626	2.407	5.544	2.269	3.592	2.765
KED	~coords + DTS + Tall shrubs	2.728	2.004	1.628	2.387	5.504	<b>2.227</b>	3.515	<b>2.494</b>
KED	~coords + DTS + Ferns	2.602	2.005	1.615	2.39	5.105	<b>2.245</b>	3.552	2.540

**Note:** Kriging methods: OK, ordinary kriging; UK, universal kriging; KED, kriging with external drift. DTS, distance to stream (m); HAS, height above stream (m); LAI, leaf area index ( $\text{m}^2$  foliage/ $\text{m}^2$  ground); DIFN, proportion visible sky; BA/ha, basal area per hectare ( $\text{m}^2/\text{ha}$ ); TPH, trees per hectare; coords, coordinates. Values in bold and underlined, bold, and bold italics indicate smallest, second smallest, and third smallest RMSE for a site, respectively. For BL13 and KM19,  $\text{DTS} = \ln(\text{DTS} + 0.1)$ ; for BL13, KM17, KM18, and KM21,  $\text{HAS} = \ln(\text{HAS} + 5)$ .

the relationships between microclimate and physical variables for stream sides separately.

As expected, LAI was negatively correlated with  $T_{\text{air}}$ , and DIFN tended to be positively correlated with  $T_{\text{air}}$ . As a measure of light energy transmittance, DIFN is an indirect measure of transmitted solar radiation, a key driver of the thermal microclimate. Areas with little overstory cover or lesser topographic shading are exposed to greater solar insolation, which results in higher maximum air temperatures than in those areas with dense canopies or, depending on channel orientation, strong topographic relief. In our study, reaches with steep streamside slope tended toward greater DIFN values than reaches with moderate streamside slope, indicating a greater amount of light reaching the understory, which resulted in higher percent cover of understory vegetation layers at reaches with steep streamside slope. Microclimate responds to whichever source of cover predominates, showing an increased sensitivity to shrub cover as overstory cover decreases. Thus, covariates describing understory vegetation cover are more important in reaches with large DIFN values. In our study, reaches with large DIFN values coincided with the reaches that have steep streamside slopes. However, this may not be true in general.

### Kriging

KED outperformed OK and UK at almost all reaches, and HAS and DTS were the most important covariates in the models. KED assumes a linear relationship between the variable of interest and the covariate. If this assumption is not met, transformations of the covariate should be tested (Bourennane et al. 2000). Log transformations of DTS and HAS improved the predictions of  $T_{\text{air}}$  in terms of RMSE for some of the sites. An improvement in the linear relationship of the log-transformed variable with  $T_{\text{air}}$  was generally reflected in an increase of Pearson's correlation coefficient (Table 3). Hudson and Wackernagel (1994) suggested that covariates

should only be used as external drift if they are highly linearly correlated with the variable of interest. If this is not the case, co-kriging, where a model for the cross-variograms between the different variables is fitted, should be preferred over KED.

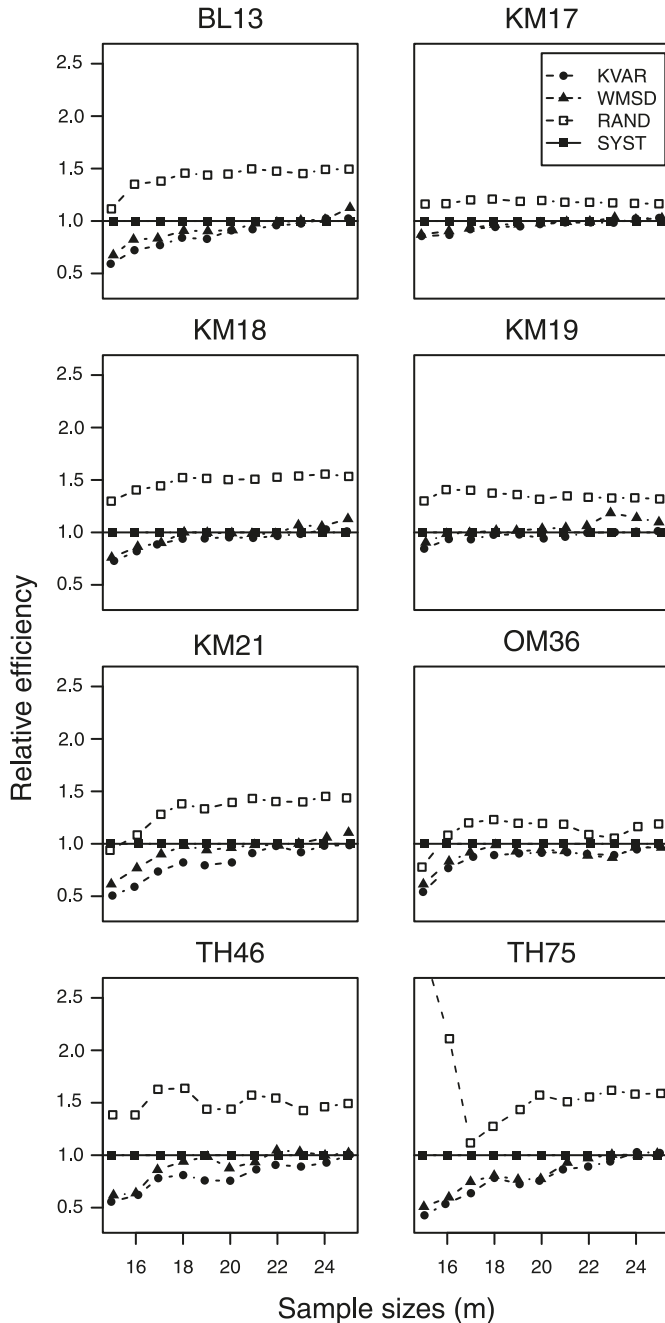
In our study, DTS outperformed HAS as external drift when channels were more steeply incised (Tables 1 and 2). This suggests that the linear relationship between  $T_{\text{air}}$  and DTS tended to be stronger on steep sites (streamside slope  $\geq 30\%$ ) than the relationship between  $T_{\text{air}}$  and HAS; the opposite was true for sites with gentler streamside slope ( $<30\%$ ).

We found that including auxiliary information with a KED model improved the predictions compared with OK and UK models, consistent with the results reported by Goovaerts (2000), Bourennane and King (2003), and van de Kasstele et al. (2009). Of the available covariates, DTS and HAS and their log transformations generally had the largest correlation coefficients with  $T_{\text{air}}$ . Bourennane and King (2003) examined whether it is necessary to use all available covariates in the KED models or whether the use of the most correlated covariate is sufficient. For their data, they found that using two external drifts resulted in more precise predictions of the variable of interest compared with using only one external drift. We found that including more than one external drift can improve predictions in terms of RMSE. However, for some of our reaches, the incremental improvement was so small that one may prefer to choose the more parsimonious model with only one external drift. At points where observations are sparse, predictions can be improved substantially by the inclusion of covariates (Bourennane et al. 2000; van de Kasstele et al. 2009).

UK with quadratic trend resulted in very good  $T_{\text{air}}$  predictions in terms of RMSE for two sites (OM36 and TH75) that exhibited a very typical  $T_{\text{air}}$  pattern for all four transects, where  $T_{\text{air}}$  was smallest at the stream center and constantly increased with increasing DTS. This pattern was not as dis-



**Fig. 2.** Relative efficiency of the sample patterns KVAR (solid circles), WMSD (open squares), RAND (open squares), and SYST (solid squares) for sample sizes  $m = 15$  to 25 for the eight stream reaches. See Table 1 for descriptions of stream reaches.



tinct on the other sites. UK with a quadratic trend was sufficient for predicting  $T_{air}$  when this type of pattern was observed. However, in absence of this pattern, UK is expected to perform worse than KED, because any spatial trend will be revealed best by defining perpendicular distance to the stream rather than distance to an arbitrary, fixed point. OK worked well when no obvious trend of  $T_{air}$  existed (e.g., KM17), so that the use of a global mean for the predictions was adequate.

We examined only the relationship of the available covari-

ates with  $T_{air}$ . However, other microclimate variables such as soil temperature and relative humidity are also of importance for ecological processes, habitat suitability, and biodiversity. Mean minimum relative humidity showed high negative correlation with  $T_{air}$ , with Pearson's correlation coefficient ranging between  $-0.68$  and  $-0.91$  for six of the sites. Smaller correlation, but still significant at the 5% level, was observed at the remaining two sites ( $-0.27$  and  $-0.48$ ). Whether the different microclimate variables respond differently to the available covariates and whether the relationships among the microclimate variables could be used to reduce sampling efforts could be examined. It is, for example, of interest whether relative humidity has to be measured at all locations where air temperature is measured.

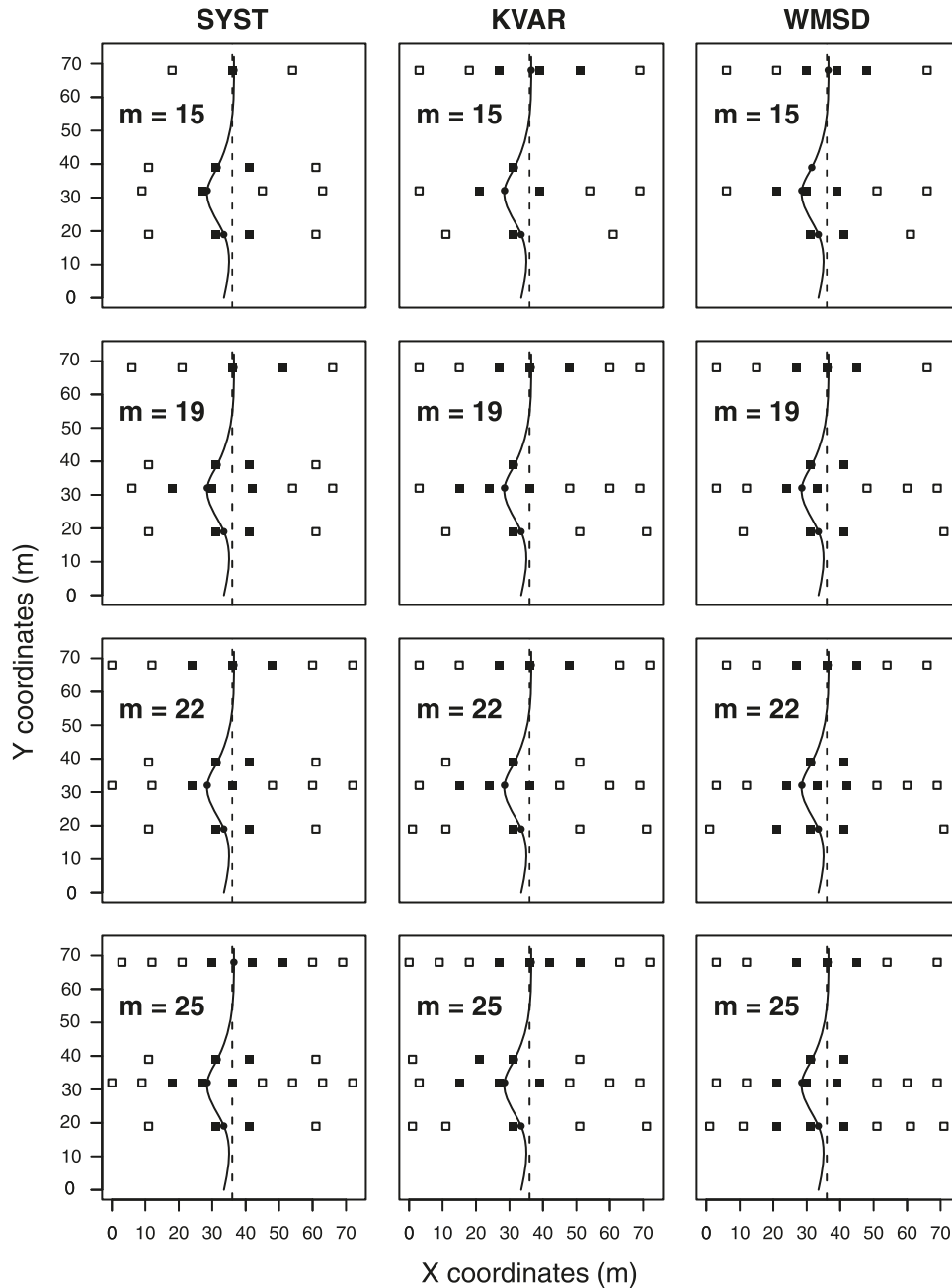
**Optimization of sampling locations**

Because of the large variability among the eight reaches, the efficiency gain of optimizing the sampling locations compared with a systematic sample was not identical for all eight reaches. Nevertheless, the results show that the optimization increased the efficiency in terms of the mean kriging variance most for smaller sample sizes (Fig. 2). This is due to WMSD and KVAR for smaller sample sizes resulting in a high density of sample points on three of the four transects, whereas the sample points for SYST were evenly spread across all four transects, thus not necessarily covering the whole range of the transects. With increasing sample size  $m$ , SYST improved compared with WMSD and KVAR, because SYST resulted in a sample being evenly spread across all four transects while providing a density of sample points along each transect similar to WMSD and KVAR, for which sample points were added to the fourth transect with increasing  $m$ . This suggests that for smaller sample sizes, it is more efficient to focus the sampling effort on fewer transects than to spread the samples across multiple transects.

Both KVAR and WMSD tended to result in fewer transects with a denser distribution of sample points than SYST, which can be attributed to the presence of anisotropy in the  $T_{air}$  data, presumably due to the variability from stream to upslope being greater than the variability along the stream. Anisotropy has considerable influence on the optimized sample patterns (van Groenigen et al. 1999). When the data are stationary, optimization of sampling locations based on the kriging variance typically results in a sample pattern similar to a triangular equilateral grid, whereas the optimized sample patterns in the presence of anisotropy lean towards larger distances between transects than between points within a transect (van Groenigen et al. 1999).

The KVAR method of optimization of sample patterns described here demands prior knowledge of the spatial variation model (variogram), implying that the optimized sample patterns are only optimal if the model assumptions used for the kriging methods are valid (Brus and Heuvelink 2007). We estimated the partial sill, range, and nugget parameters for each reach based on all observations available for the reach ( $50 \leq n \leq 65$ ) and assumed these parameter estimates to be correct. At least 50 observations are recommended for variogram estimation, but around 300 observations are preferred (Webster and Oliver 2001, p. 85). Therefore, it can be assumed that our kriging results and optimized sample patterns could be improved if more resources were put into estimating

**Fig. 3.** SYST, KVAR, and WMSD sample patterns for stream reach BL13 for  $m = 15, 19, 22,$  and  $25$ : solid square, sample location within 15 m of stream; open square, distance to stream of sample location is greater than 15 m.



the variogram parameters. However, because parameter estimation was not the focus of this study, we did not explore many different models.

Optimization based on the kriging variance can only be applied if a variogram can be assumed by either estimation from sampled data or inference from earlier surveys. If this is not possible, other optimization criteria (e.g., minimizing the mean of shortest distance criterion, WMSD criterion) that do not require the knowledge of variogram parameters may provide better optimization results (van Groenigen et al. 1999). KVAR had slightly larger RE values than WMSD for five of the reaches and smaller RE values than WMSD for the remaining three reaches. This confirms that optimization

criteria not dependent on variogram estimation such as the WMSD criterion can be valid alternatives to methods such as KVAR (Fig. 2).

The kriging models did not converge for some sample patterns with sample sizes  $m < 15$ , and we wanted to have at least as many evaluation points ( $n - m$ ) as sampling points ( $m$ ). Therefore, we were limited to examining sample sizes ranging between  $m = 15$  and  $25$  because of the small data sets for each of the eight reaches ( $50 \leq n \leq 65$ ). Hence, this study does not allow information about the performance of the different sample patterns and kriging methods for sample sizes larger 25 or smaller 15. Cost models of the different sample patterns were not examined.

Can. J. For. Res. Downloaded from www.nrcresearchpress.com by OREGON STATE UNIVERSITY on 05/06/11 For personal use only.

## Conclusions

We show the potential of using geostatistical tools for predicting microclimate variables, in particular  $T_{\text{air}}$ , in forested riparian zones. Strong correlations were found between  $T_{\text{air}}$  and DTS and HAS. Statistically significant correlations between  $T_{\text{air}}$  and canopy cover variables and over- and under-story vegetation attributes have been found for some reaches. However, these correlations are not consistent across reaches.

KED provided better results in terms of RMSE than OK or UK when either DTS or HAS were used as external drift. HAS and DTS or their log transformations were the most useful covariates for KED. For steep sites (>30%), DTS was more important as external drift than HAS. The opposite was true for sites with slope less than 30%. Using more than one external drift by including covariates that describe the percent cover of the over- or under-story vegetation can improve the prediction results, although consistent improvements across reaches were not shown. Whichever source of cover predominates at a reach explains the most variation in the model.

The kriging variance and the WMSD criterion were used to optimize the sample pattern with the simulated annealing algorithm. We found that the KVAR- and WMSD-optimized sample patterns have the potential to improve the efficiency of predicting  $T_{\text{air}}$  in terms of the mean kriging variance compared with systematic sample patterns (SYST). This is especially true for smaller sample sizes ( $m < 20$ ), which can be attributed to denser samples along a subset of the four transects for KVAR and WMSD compared with less intense samples along all four transects for SYST.

The variogram parameters were estimated with 50 to 65 data points for the eight reaches. Because the performance of the kriging models and the KVAR optimization strongly depend on the estimated variogram parameters, it can be expected that improved variogram estimation based on more data points may improve the results over those presented.

The findings of our study can help researchers attempting to monitor and map microclimate conditions in riparian areas in choosing relevant auxiliary information and optimal sample patterns for long-term monitoring efforts.

## Acknowledgments

Any use of trade, product, or firm names is for descriptive purposes only and does not imply endorsement by the U.S. Government. We would like to thank Chris Sheridan and Dede Olson for their feedback on an early version of the manuscript, two anonymous reviewers and the Associate Editor for their helpful comments, and Kevin Boston and John Sessions for suggestions about the parameterization of the simulated annealing algorithm. Special thanks go to Theresa Marquardt, Timothy Drake, and Andrew Neill, who collected the data and answered many questions concerning the data.

## References

- Adams, J. 2007. Vegetation–climate interaction. How vegetation makes the global environment. Praxis Publishing Ltd., Chichester, UK.
- Anderson, P.D., Larson, D.J., and Chan, S.S. 2007. Riparian buffer and density management influences on microclimate of young headwater forests of western Oregon. *For. Sci.* **53**(2): 254–269.
- Bourennane, H., and King, D. 2003. Using multiple external drifts to estimate a soil variable. *Geoderma*, **114**(1–2): 1–18. doi:10.1016/S0016-7061(02)00338-5.
- Bourennane, H., King, D., and Couturier, A. 2000. Comparison of kriging with external drift and simple linear regression for predicting soil horizon thickness with different sample densities. *Geoderma*, **97**(3–4): 255–271. doi:10.1016/S0016-7061(00)00042-2.
- Brosfokske, K.D., Chen, J., Naiman, R.J., and Franklin, J.F. 1997. Harvesting effects on microclimatic gradients from small streams to uplands in western Washington. *Ecol. Appl.* **7**(4): 1188–1200. doi:10.1890/1051-0761(1997)007[1188:HEOMGF]2.0.CO;2.
- Brus, D.J., and Heuvelink, G.B.M. 2007. Optimization of sample patterns for universal kriging of environmental variables. *Geoderma*, **138**(1–2): 86–95. doi:10.1016/j.geoderma.2006.10.016.
- Chen, J., Franklin, J.F., and Spies, T.A. 1993. Contrasting microclimates among clearcut, edge, and interior of old-growth Douglas-fir forest. *Agric. For. Meteorol.* **63**(3–4): 219–237. doi:10.1016/0168-1923(93)90061-L.
- Chen, J., Franklin, J.F., and Spies, T.A. 1995. Growing-season microclimatic gradients from clearcut edges into old-growth Douglas-fir forests. *Ecol. Appl.* **5**(1): 74–86. doi:10.2307/1942053.
- Chen, J., Saunders, S.C., Crow, T.R., Naiman, R.J., Brosfokske, K.D., Mroz, G.D., Brookshire, B.L., and Franklin, J.F. 1999. Microclimate in forest ecosystem and landscape ecology. Variations in local climate can be used to monitor and compare the effects of different management regimes. *Bioscience*, **49**(4): 288–297. doi:10.2307/1313612.
- Cissel, J.H., Anderson, P.D., Olson, D., Puettmann, K.P., Berryman, S., Chan, S.S., and Thompson, C. 2006. BLM density management and riparian buffer study: establishment report and study plan. U.S. Geological Survey, Scientific Investigations Report 2006-5087.
- de Grijter, J.J., Brus, D.J., Bierkens, M.F.P., and Knotters, M. 2006. Sampling for natural resource monitoring. Springer, Heidelberg, Germany.
- Dong, J., Chen, J., Brosfokske, K.D., and Naiman, R.J. 1998. Modelling air temperature gradients across managed small streams in western Washington. *J. Environ. Manage.* **53**(4): 309–321. doi:10.1006/jema.1998.0217.
- Geiger, R., Aron, R.H., and Todhunter, P. 2003. The climate near the ground. Rowman & Littlefield Publishers, Inc., Lanham, Maryland.
- Gomi, T., Moore, R.D., and Dhakal, A.S. 2006. Headwater stream temperature response to clear-cut harvesting with different riparian treatments, coastal British Columbia, Canada. *Water Resour. Res.* **42**: W08437. doi:10.1029/2005WR004162.
- Goovaerts, P. 1997. Geostatistics for natural resources evaluation. Oxford University Press, New York.
- Goovaerts, P. 2000. Geostatistical approaches for incorporating elevation into the spatial interpolation of rainfall. *J. Hydrol. (Amst.)*, **228**(1–2): 113–129. doi:10.1016/S0022-1694(00)00144-X.
- Hagan, J.M., and Whitman, A.A. 2000. Microclimate changes across upland and riparian clearcut forest boundaries in Maine. Manomet Center for Conservation Sciences, Brunswick, Maine, Mosaic Science Notes 2000-4. Available at <http://www.manometmaine.org/publications.html> [accessed 18 March 2011].
- Hengl, T. 2007. A practical guide to geostatistical mapping of environmental variables. EUR 22904 EN, Scientific and Technical Research Series, Office for Official Publications of the European Communities, Luxembourg.
- Hibbs, D.E., and Bower, A.L. 2001. Riparian forests in the Oregon Coast Range. *For. Ecol. Manage.* **154**(1–2): 201–213. doi:10.1016/S0378-1127(00)00623-X.

- Hudson, G., and Wackernagel, H. 1994. Mapping temperature using kriging with external drift: theory and an example from Scotland. *Int. J. Climatol.* **14**(1): 77–91. doi:10.1002/joc.3370140107.
- Lark, R.M., and Webster, R. 2006. Geostatistical mapping of geomorphic variables in the presence of trend. *Earth Surf. Process. Landf.* **31**(7): 862–874. doi:10.1002/esp.1296.
- Li, Y., and Chan Hilton, A.B. 2005. Reducing spatial sampling in long-term groundwater monitoring networks using ant colony optimization. *Int. J. Comput. Intell. Res.* **1**(1): 19–28.
- Li, Y., and Chan Hilton, A.B. 2007. Optimal groundwater monitoring design using an ant colony optimization paradigm. *Environ. Model. Softw.* **22**(1): 110–116. doi:10.1016/j.envsoft.2006.05.023.
- Moore, R.D., Spittlehouse, D.L., and Story, A. 2005. Riparian microclimate and stream temperature response to forest harvesting: a review. *J. Am. Water Resour. Assoc.* **41**(4): 813–834.
- Müller, W.G. 2007. *Collecting spatial data. Optimum design of experiments for random fields.* Springer, Berlin, Germany.
- Naiman, R.J., Bilby, R.E., and Bisson, P.A. 2000. Riparian ecology and management in the Pacific coastal rain forest. *Bioscience*, **50** (11): 996–1011. doi:10.1641/0006-3568(2000)050[0996:REAMIT]2.0.CO;2.
- Olson, D.H., Anderson, P.D., Frissell, C.A., Welsh, H.H., Jr, and Bradford, D.F. 2007. Biodiversity management approaches for stream-riparian areas: perspectives for Pacific Northwest headwater forests, microclimates, and amphibians. *For. Ecol. Manage.* **246**(1): 81–107. doi:10.1016/j.foreco.2007.03.053.
- Pabst, R.J., and Spies, T.A. 1998. Distribution of herbs and shrubs in relation to landform and canopy cover in riparian forests of coastal Oregon. *Can. J. Bot.* **76**(2): 298–315. doi:10.1139/cjb-76-2-298.
- R Development Core Team. 2009. R: a language and environment for statistical computing. R Foundation for Statistical Computing, Vienna, Austria. Available at <http://www.R-project.org>.
- Rambo, T.R., and North, M.P. 2008. Spatial and temporal variability of canopy microclimate in a Sierra Nevada riparian forest. *Northwest Sci.* **82**(4): 259–268. doi:10.3955/0029-344X-82.4.259.
- Reeves, C.R. 1993. *Modern heuristic techniques for combinatorial problems.* John Wiley and Sons, Inc., New York.
- Ribeiro, P.J. , Jr., and Diggle, P.J. 2001. geoR: a package for geostatistical analysis. *R News*, **1**(2): 15–18.
- Richardson, J.S., Naiman, R.J., Swanson, F.J., and Hibbs, D.E. 2005. Riparian communities associated with Pacific Northwest headwater streams: assemblages, processes, and uniqueness. *J. Am. Water Resour. Assoc.* **41**(4): 935–947.
- Russell, G., Jarvis, P.G., and Monteith, J.L. 1989. Absorption of radiation by canopies and stand growth. *In* Plant canopies: their growth, form and function. *Edited by* G. Russell, B. Marshall, and P.G. Jarvis. Cambridge University Press, New York. pp. 21–39.
- Rykken, J.J., Chan, S.S., and Moldenke, A.R. 2007. Headwater riparian microclimate patterns under alternative forest management treatments. *For. Sci.* **53**: 270–280.
- Stein, A., and Ettema, C. 2003. An overview of spatial sampling procedures and experimental design of spatial studies for ecosystem comparisons. *Agric. Ecosyst. Environ.* **94**(1): 31–47. doi:10.1016/S0167-8809(02)00013-0.
- van de Kasstele, J., Stein, A., Dekkers, A.L.M., and Velders, G.J.M. 2009. External drift kriging of NO<sub>x</sub> concentrations with dispersion model output in a reduced air quality monitoring network. *Environ. Ecol. Stat.* **16**(3): 321–339. doi:10.1007/s10651-007-0052-x.
- van Groenigen, J.W., and Stein, A. 1998. Constrained optimization of spatial sampling using continuous simulated annealing. *J. Environ. Qual.* **27**(5): 1078–1086. doi:10.2134/jeq1998.00472425002700050013x.
- van Groenigen, J.W., Siderius, W., and Stein, A. 1999. Constrained optimisation of soil sampling for minimisation of the kriging variance. *Geoderma*, **87**(3–4): 239–259. doi:10.1016/S0016-7061(98)00056-1.
- van Groenigen, J.W., Pieters, G., and Stein, A. 2000. Optimizing spatial sampling for multivariate contamination in urban areas. *Environmetrics*, **11**: 227–244. doi:10.1002/(SICI)1099-095X(200003/04)11:2<227::AID-ENV404>3.0.CO;2-#.
- Vanwalleghem, T., and Meentemeyer, R.K. 2009. Predicting forest microclimate in heterogeneous landscapes. *Ecosystems (N.Y.)*, **12** (7): 1158–1172. doi:10.1007/s10021-009-9281-1.
- Walvoort, D., Brus, D., and de Gruijter, J. 2010. An R package for spatial coverage sampling and random sampling from compact geographical strata by k-means. *Comput. Geosci.* **36**(10): 1261–1267. doi:10.1016/j.cageo.2010.04.005.
- Webb, B.W., Hannah, D.M., Moore, R.D., Brown, L.E., and Nobilis, F. 2008. Recent advances in stream and river temperature research. *Hydrol. Process.* **22**(7): 902–918. doi:10.1002/hyp.6994.
- Webster, R., and Oliver, M.A. 2001. *Geostatistics for environmental scientists.* Statistics in Practice, Wiley, Chichester.
- Welsh, H.H., Jr., Hodgson, G.R., and Karraker, N.E. 2005. Influences of the vegetation mosaic on riparian and stream environments in a mixed forest–grassland landscape in “Mediterranean” northwestern California. *Ecography*, **28**(4): 537–551. doi:10.1111/j.0906-7590.2005.04025.x.